Electronic Supplementary Material (ESI) for Journal of Materials Chemistry C.

ELECTRONIC SUPPORTING INFORMATION

Antiaromatic Non-Alternant Heterocyclic Compounds as Molecular Wires

Edmund Leary,*[a] Carlos Roldán-Piñero,[b] Rocío Rico-Sánchez-Mateos [b] and Linda A. Zotti*[b,c]

a Fundación IMDEA Nanociencia, E-28049 Madrid, Spain.
E-mail: edmund.leary@imdea.org
b Departamento de Física Teórica de la Materia Condensada, Universidad Autónoma de Madrid, E-28049 Madrid, Spain.
E-mail: linda.zotti@uam.es
c Condensed Matter Physics Center (IFIMAC) and Instituto Nicolás Cabrera (INC), Universidad Autónoma de Madrid, E- 28049 Madrid, Spain

TABLE OF CONTENTS

1. DTP atom numbering

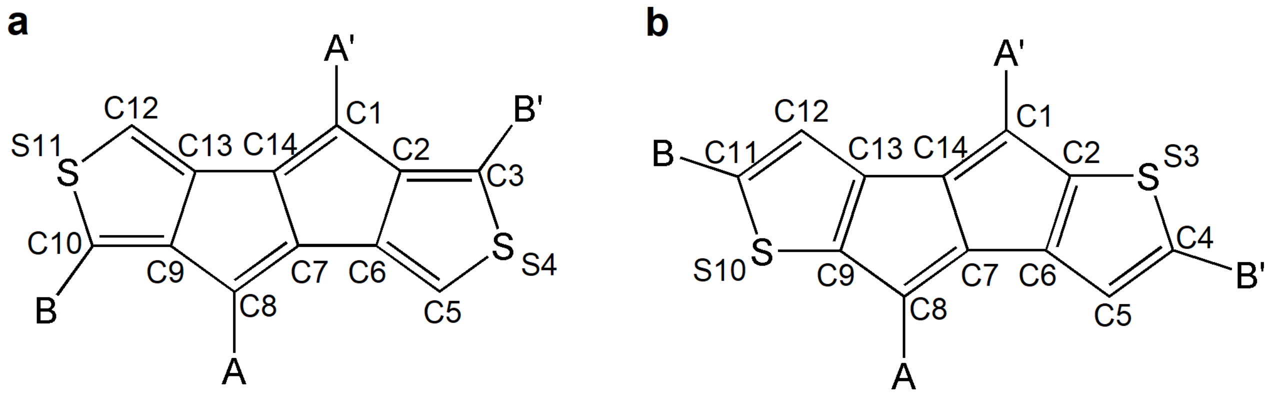

Figure S1: figure showing the numbering of each site in the DTP cores.

2. Gas-phase energies

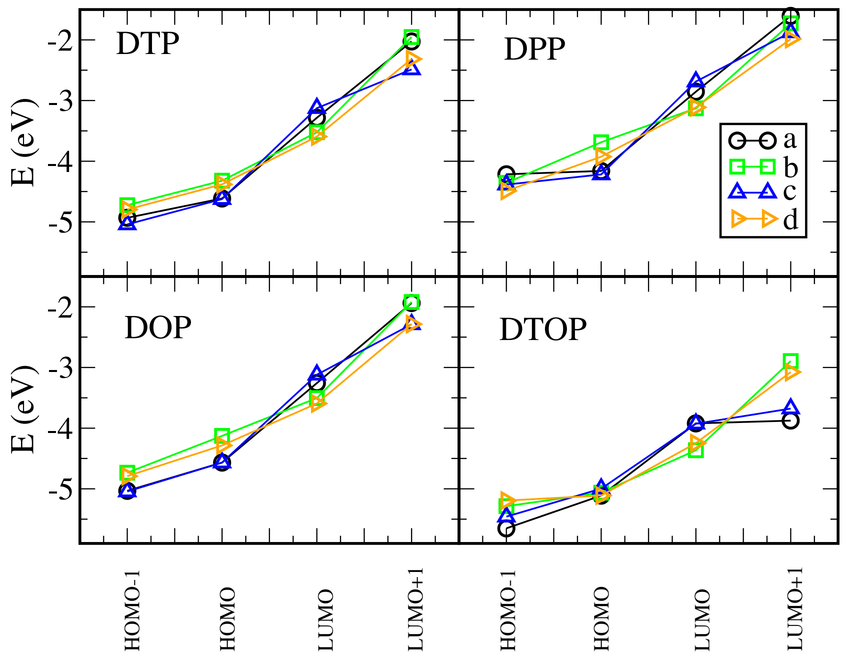

Figure S2: Energetic positions of four selected molecular orbitals in the gas phase for all compounds.

3. Gas-phase Orbitals

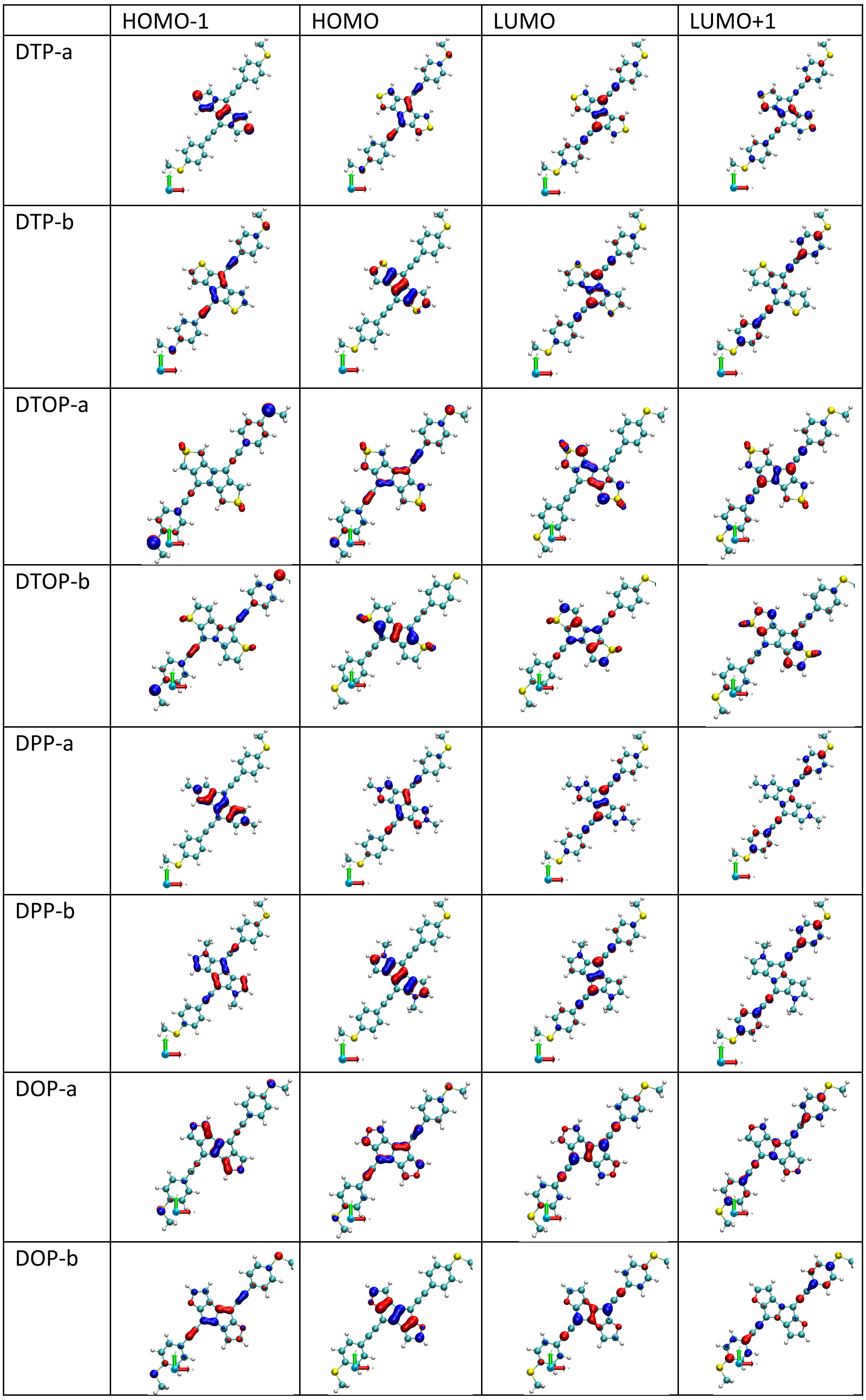

Figure S3: Spatial distribution of the gas-phase molecular orbitals in the a and b isomers for all compounds.

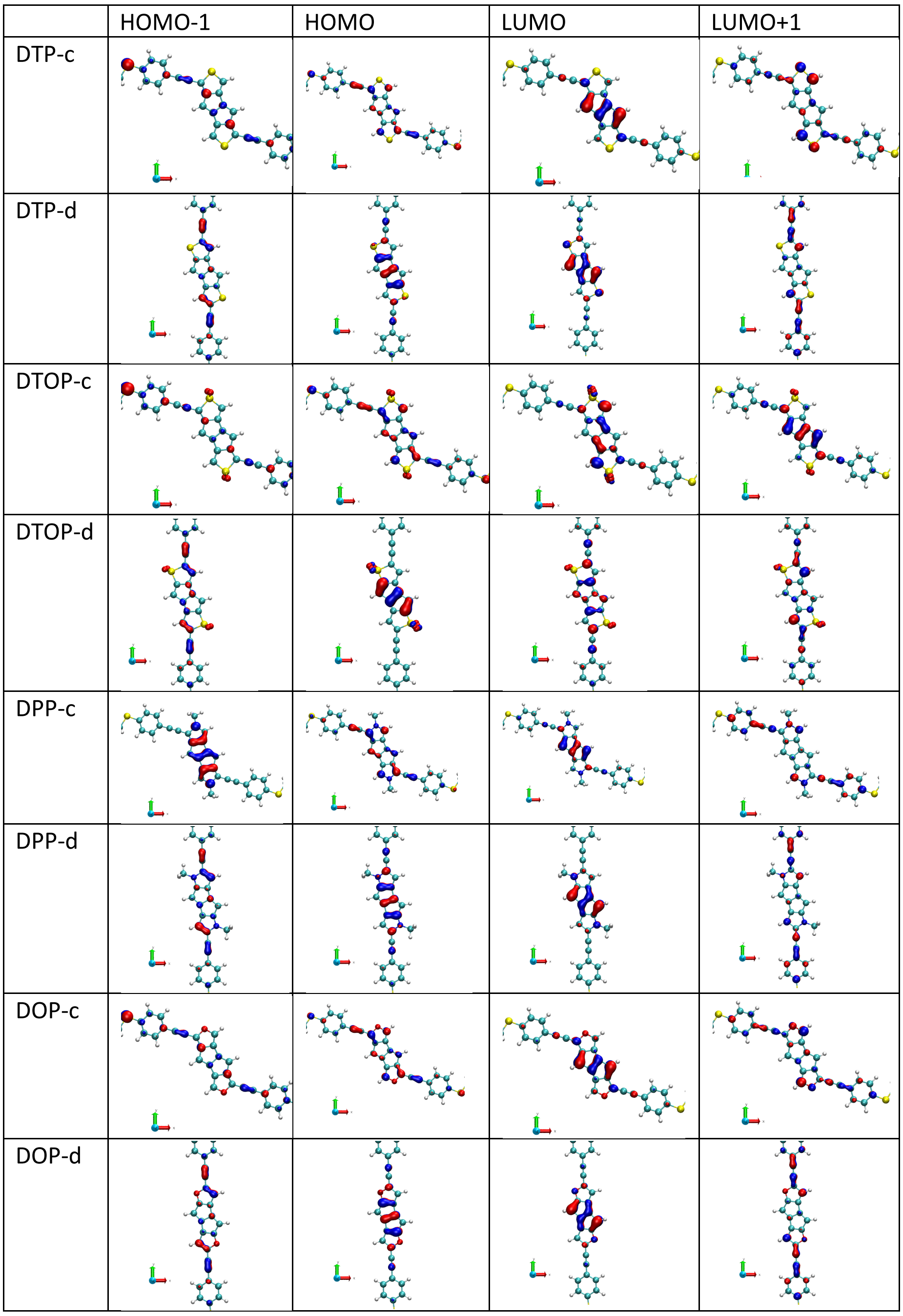

Figure S4: Spatial distribution of the gas-phase molecular orbitals in the c and d isomers for all compounds.

4. NICS(1)$_{iso}$-calculations.

In the table below, we report the nucleus independent chemical shifts (NICS) values obtained for all compounds analyzed in the main text, averaged over the two outer heterocycles and the two inner 5-membered rings (values are given in ppm). Negative NICS values indicate a diatropic ring current (associated with aromatic character) while positive NICS values indicate a paratropic ring current (associated with antiaromatic character. The NICS values were obtained by calculations based on Gaussian 09, using B3LYP/6-31G(d) level of theory. The dummy atoms were placed at a distance of 1 Å from the center of each ring.

		Outer heterocycle ring	Inner 5-membered ring
a structures	DTP	-5.69	0.41
	DPP	-5.39	2.90
	DOP	-6.16	-0.14
	DTOP	-2.17	-3.21
b structures	DTP	-3.74	14.77
	DPP	0.14	24.11
	DOP	-3.80	20.36
	DTOP	-4.02	7.91
c structures	DTP	-5.67	1.31
	DPP	-4.64	3.56
	DOP	-5.47	0.67
	DTOP	-2.32	-3.02
d structures	DTP	-3.96	19.72
	DPP	-1.57	19.83
	DOP	-2.98	23.39
	DTOP	-3.91	6.65

5. Gap-corrected DFT-based transmission curves and tight-binding calculations

In panel (a) of figure S5, we show the transmission curves for the DTP compounds obtained using the same DFT-based procedure as for the curves in Fig.4 of the main text, but applying a correction to the HOMO-LUMO gap. This was achieved via the DFT+ Σ technique (see the section "computational details").

In panel (b), we report the transmission curves obtained by a tight-binding model. For this, the following parameters were used: t_1 = -1.5 eV, t_2 = -2.7 eV, t_3 = -3.0, t_a = -2.5 eV, t_S = -2 eV e_C = 0, e_S = -2.9 eV, where t_1, t_2, t_3 are the couplings corresponding to single, double and triple bonds, respectively, while t_a is the coupling within the benzene rings, and t_S is the coupling to the sulfur within the thiophene.

We set the C-S coupling to the benzene sulfur equal to t_1. The parameters e_C and e_S are the on-site energies for the C and S atoms. Finally, the coupling to the leads was set to -0.5 eV. It can be observed that the tight binding reproduces the behavior predicted by DFT quite closely.

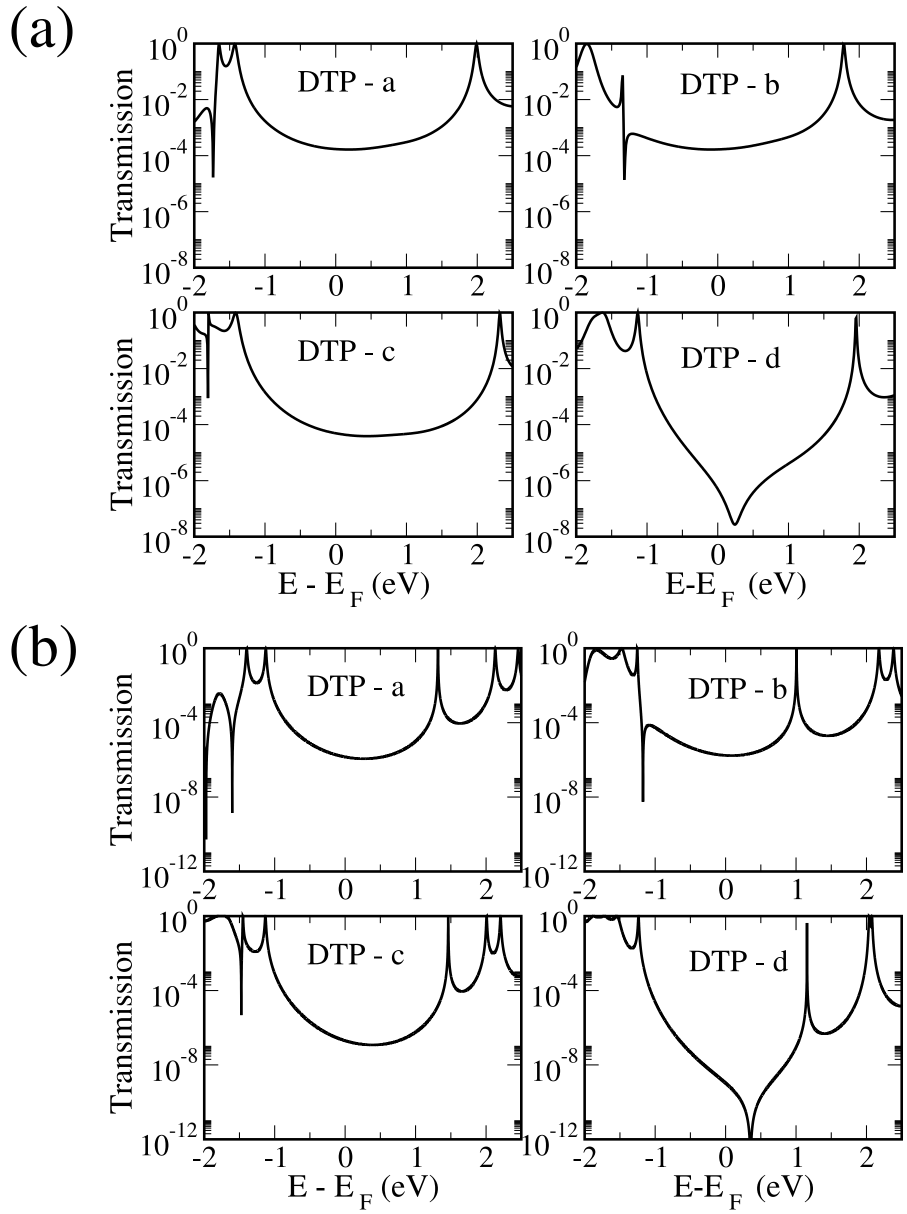

Figure S5: (a) HOMO-LUMO gap -corrected transmission curves; b) tight-binding transmission curves.

6. Transport calculations for additional isomers.
The figure below shows the transport calculations for compounds based on two isomers which were not studied in Ref 1 and thus not considered in the main text. The isomer DTP-e shown in panel a (which shows CQI) has the same DTP core structure as DTP-c, but the position of the MeS-Ph-CC anchor groups is different (they are positioned on opposite sides of the core): this, in turn, alters the relative position of the bonds in the core versus in the anchor groups. The DTP core of DTP-f is similar to that in DTP-d, but the position of the thiophene sulfurs with respect to the pentalene core is different.

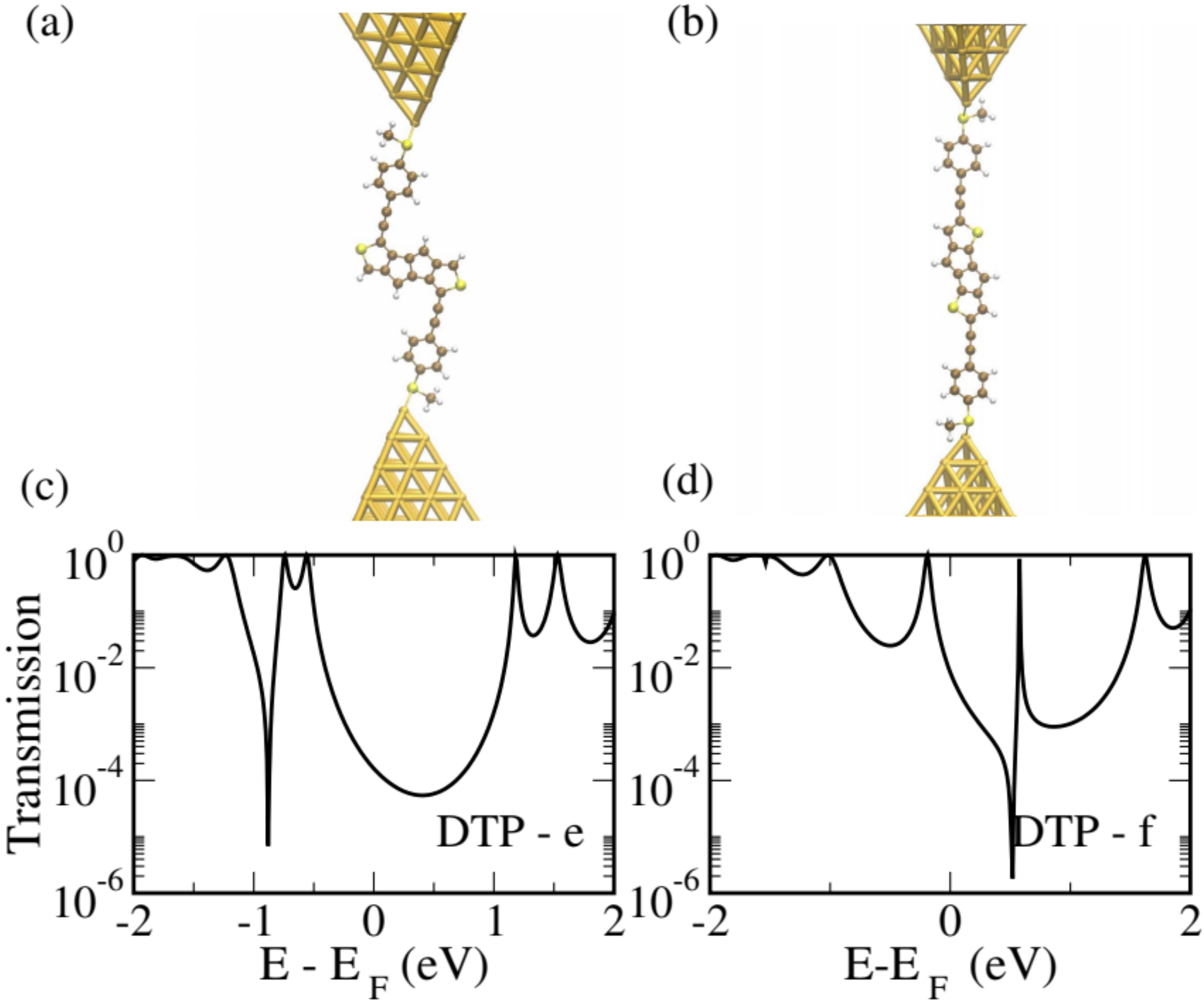

Figure S6: (a-b) Junctions based on two isomers which were not studied in Ref [1]and (c-d) corresponding transmission curves.

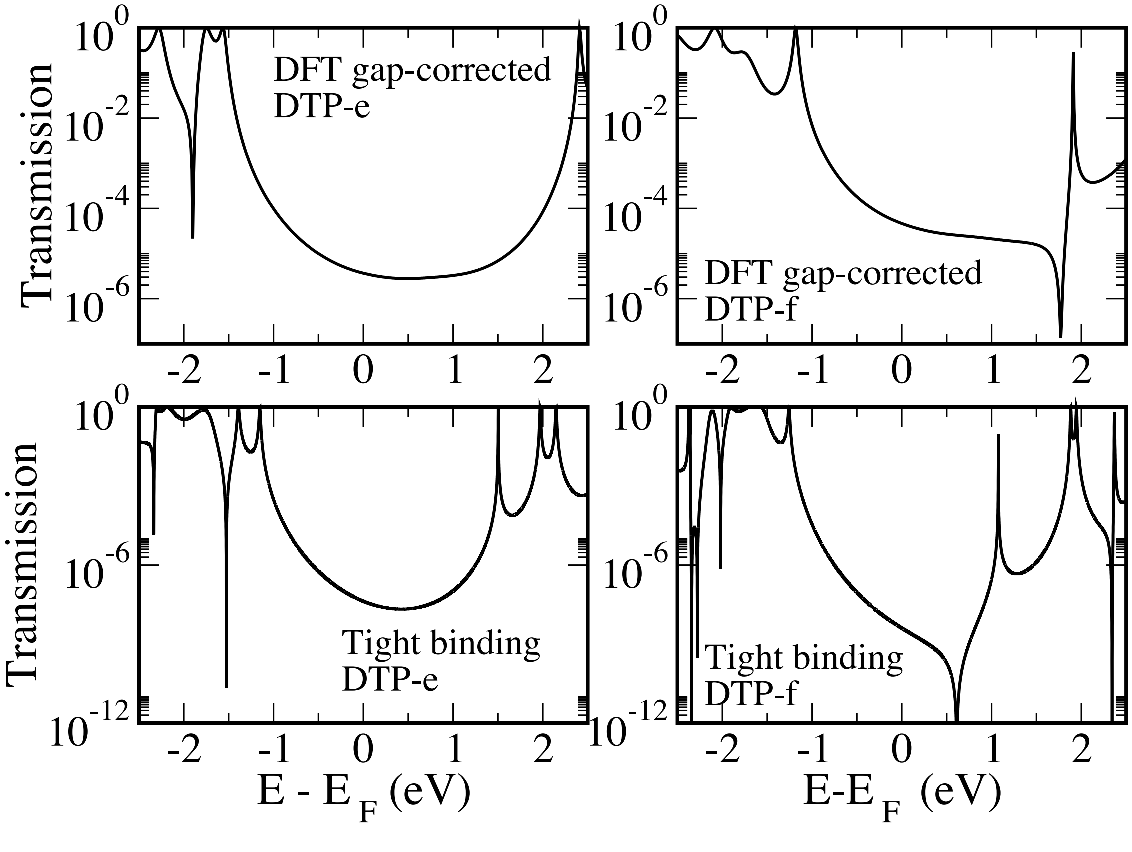

Figure S7: DFT gap corrected and tight-binding transmission curves for isomers DPT-e and DPT-f. The tight-binding parameters are the same as used for the other isomers.

Figure S6 c and d show the transmission curves obtained for the additional isomers DTP-e and DTP-f. DTP-e has the same DTP core as DTP-c but the MeS-Ph-CC anchor groups have been positioned on opposite sides of the core relative to DTP-c (i.e. they are located at C5 and C12 rather than C3 and C10). As with DTP-c, DTP-e gives rise to CQI within the HOMO–LUMO gap, however, CARs predict DQI as a consequence of not being able to draw a delocalisation pathway between the two anchor group sites (Figure S10). At first glance, this appears to suggest that CARs fail even for compounds that are not strongly antiaromatic. It is known that compounds with heteroatoms for which DQI is predicted can deviate from this prediction. This can be accounted for by considering additional resonance structures involving the heteroatoms (as described by O'Driscoll and Bryce (ref. 30 in the main text) using their extended curly arrow 2 method - ECAR-2). For DTP-e, if the anchor groups are replaced by two acceptor groups (see Figure S11) then it possible to delocalize a sulfur lone pair with both acceptor groups. According to ECAR-2, this leads to the prediction of shifted-DQI, which could fit with the results of DTP-e in Figure S6. There is, as previously mentioned, no DQI within the HOMO–LUMO gap, so *a priori* it is difficult to judge if this idea is correct. We decided, therefore, to model DTP-e using tight binding, which also allows us to break specific bonds to check what effect this has on the transmission. Figure S9 shows the TB results for the original structure (black curve). Note, we used the same parameters as for the other DTP isomers. The red curve, on the other hand, shows the result of setting the coupling to the thiophene sulfur atoms to zero (i.e. breaking the C-S thiophene bonds). In this situation, DQI now appears in the HOMO–LUMO gap, agreeing with the curly arrow prediction. Thus, when conjugation to the sulfurs is broken, agreement with CARs is restored, which provides good evidence for the idea of shifted-DQI in the framework of ECAR-2.

To verify this further, we also carried out the same procedure on DTP-c and DTP-d (setting the coupling to thiophene S sites to zero). In these cases, only slight modifications to the transmission curves can be seen, but the respective interference patterns within the HOMO–LUMO gaps do not change.

DTP-f has a similar core to DTP-b/d, but the thiophene sulfur atoms are oriented differently with respect to the pentalene core. As with DTP-d, DTP-f also produces DQI within the HOMO–LUMO gap in the DFT-based transmission curve (Figure S6 d), but this time both DFT and CARs agree. This can be explained due to the fact that there is no way to connect the substituted donor and acceptor groups via any potential path through the molecule using curly arrows, neither around the periphery of the molecule or via the C14-C7 transannular bond.

7. Additional tight-binding analysis.

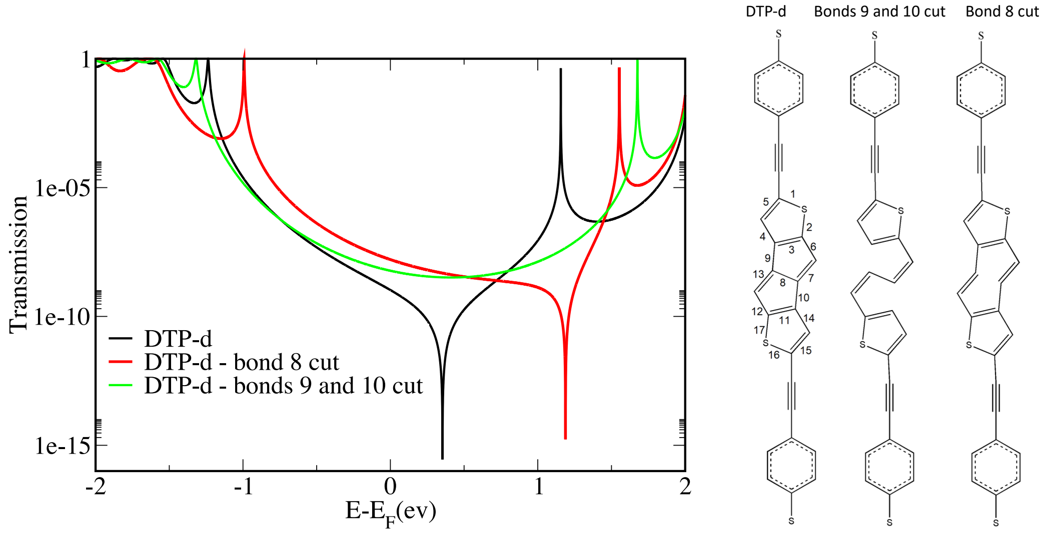

1 2 3

Figure S8: tight-binding transmission curves for DTP-d (solid black) and modified structures obtained by cutting specific bonds, as shown in the right-hand panel.

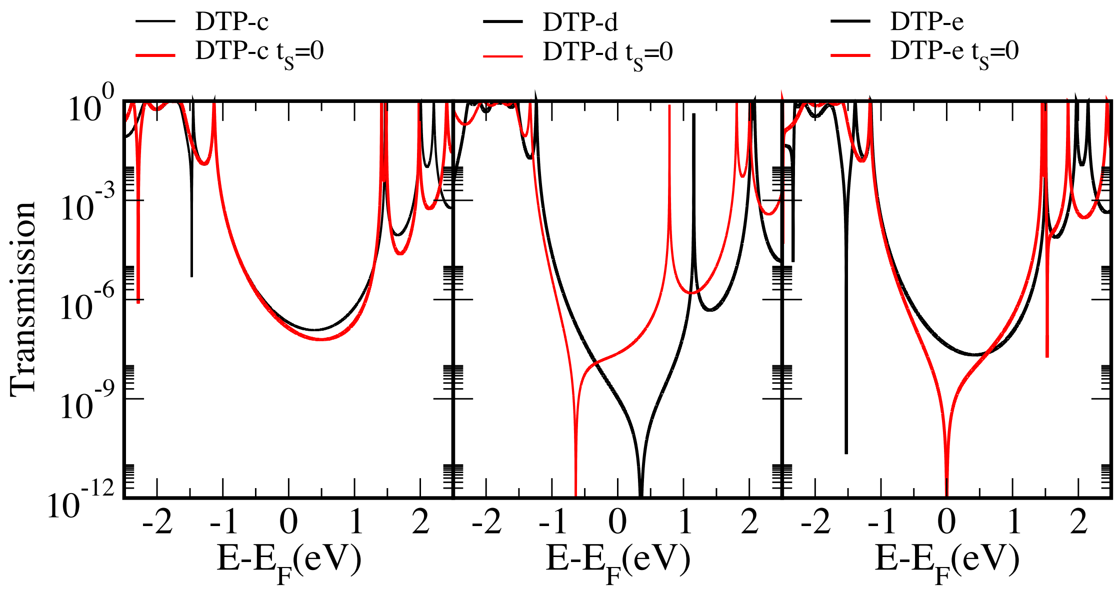

Figure S9: Additional tight binding transmission curves for a selection of isomers comparing the complete structures with those in which the coupling to the thiophene sulfur is set to zero (t_S=0)

8. Computational details:

We performed DFT-based transport calculations following the procedure described in detail in ref. [2, 3], which is based on the Turbomole code [4]. For this, a def-SVP basis set [5] and BP86 functional [6] were employed. Au-molecule-Au junctions were built by inserting the optimized structures of the gas phase molecules between two Au 20 pyramidal clusters and by performing a new optimization of the whole geometry. In this last step, the atoms in the two innermost gold layers and the molecule were relaxed while the others were kept frozen. This was followed by extending the size of each gold cluster to 63 atoms (to ensure correct charge transfer) and performing a single-point calculation on the new structure. The transport properties were then evaluated in the spirit of the Landauer formalism, after correcting the HOMO-LUMO gap with the DFT+Σ correction [3,7]. The low-bias conductance was given by $G = G_0 \tau(E_F) = G_0 \Sigma_i \tau_i(E_F)$, where G_0 is the conductance quantum $2e^2/h$, E_F is the Fermi energy, and $\{\tau_i\}$ are the transmission coefficients.

9. Curly arrows

The basic idea of the curly-arrow rules (CAR) begins with a skeletal drawing of the Lewis structure of the molecule where the formal single bonds are represented by single lines, and double and triple bonds with two or three parallel lines respectively. In its basic form, the CAR method involves looking for resonance structures which formally shift a pair of electrons from a donor (D) to an acceptor (A) group which have replaced the anchor groups at the ends of the molecule. This is essentially a representation of the delocalisation of electrons across the molecular backbone. If delocalisation is possible from D to A, constructive quantum interference (CQI) is predicted to dominate within the HOMO-LUMO gap. On the other hand, if there is no way of delocalising the electrons between D and A, DQI should dominate. We note that this theory assumes transport takes place within the HOMO-LUMO gap and that no significant charge transfer takes place which could drastically alter the bonding. For alternant molecules which can be represented by way of a bipartite lattice, this translates to the statement that connections between sites of the same sublattice will give rise to DQI whilst those between different sublattices will produce CQI. As Bryce pointed out, however, several situations can cause basic CARs to breakdown. This includes the presence of cross-conjugation, heteroatoms and non-alternant hydrocarbons. In light of this, extended-CARs (ECARs) were put forward to deal with each situation. We refer to Ref.8 for a detailed discussion of ECARs, but we note the first axiom of the ECARs is identical to CARs: “If the D lone pair can be delocalised onto A using curly arrows, CQI is expected”. ECARs have been used to explain the higher-than-expected measured conductances for compounds where DQI around the Fermi level, and hence a low conductance, was anticipated.

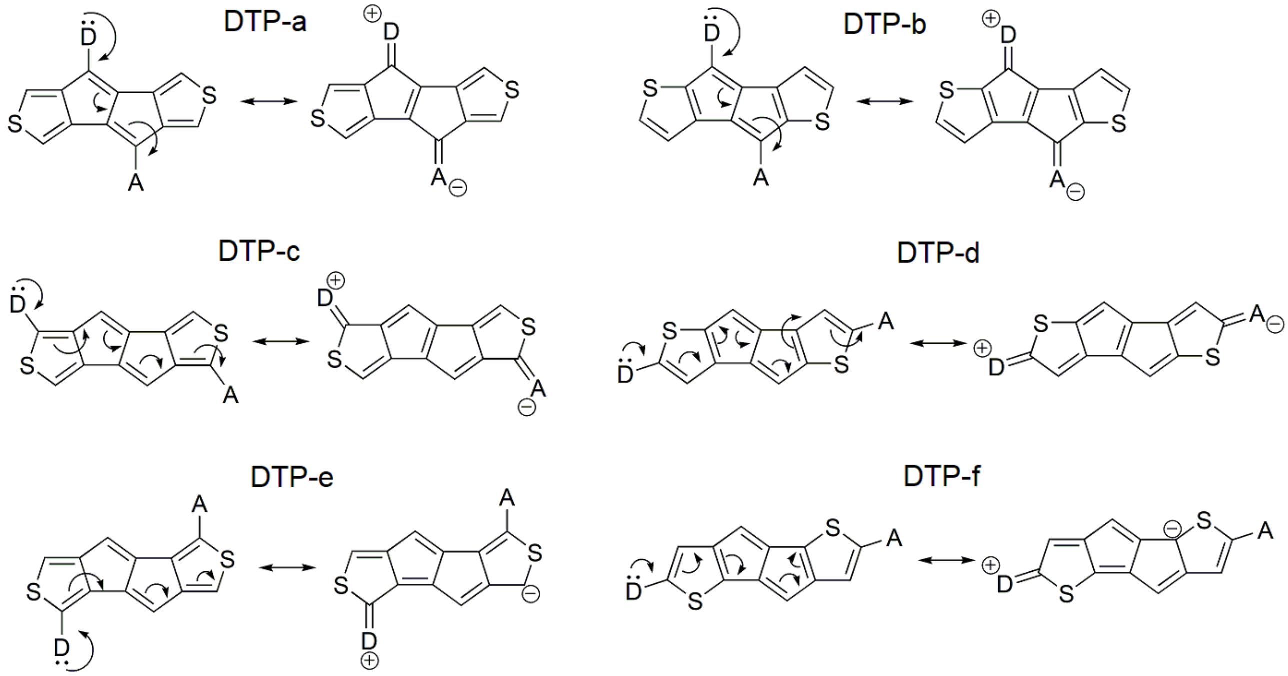

Figure S10:Application of basic curly-arrow rules to compounds DTP-a to DTP-f. In each case, the CC-Ph-SMe anchor groups have been replaced by a donor (D) and an accepter (A) group. If it is possible to draw curly arrows connecting the lone pair on D to the accepte er A, constructive interference is predicted. If not, DQI should appear.

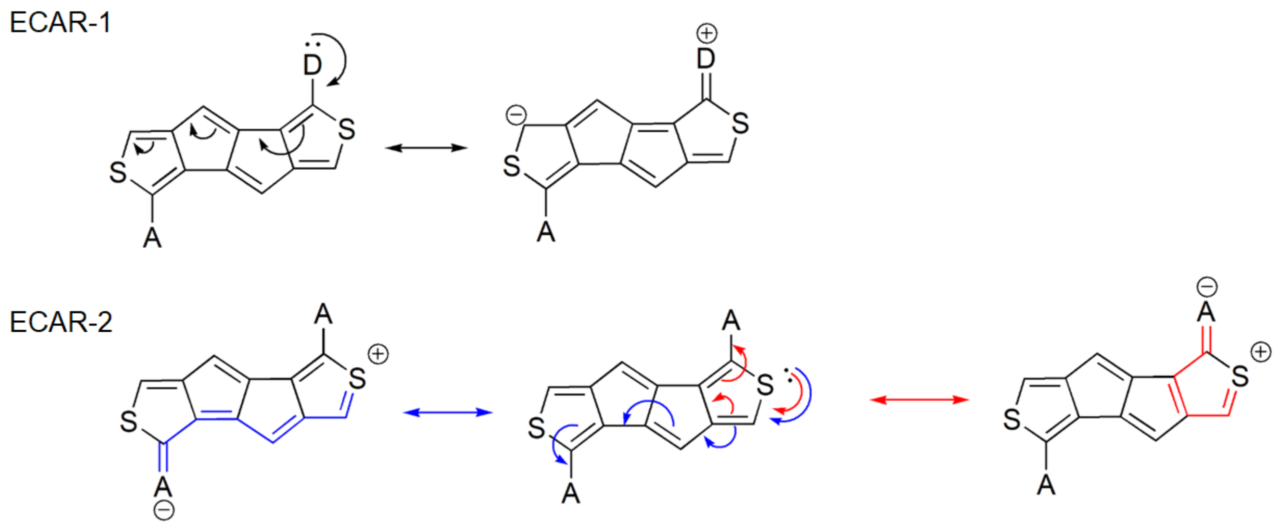

Figure S11: Application of extended curly-arrow rules to DTP-e.

10. Graphical method

The figure below shows the MST diagrams obtained for DTP-d, considering a maximum of 3 one-site loops. Below each diagram, the corresponding contribution to the equation is given.

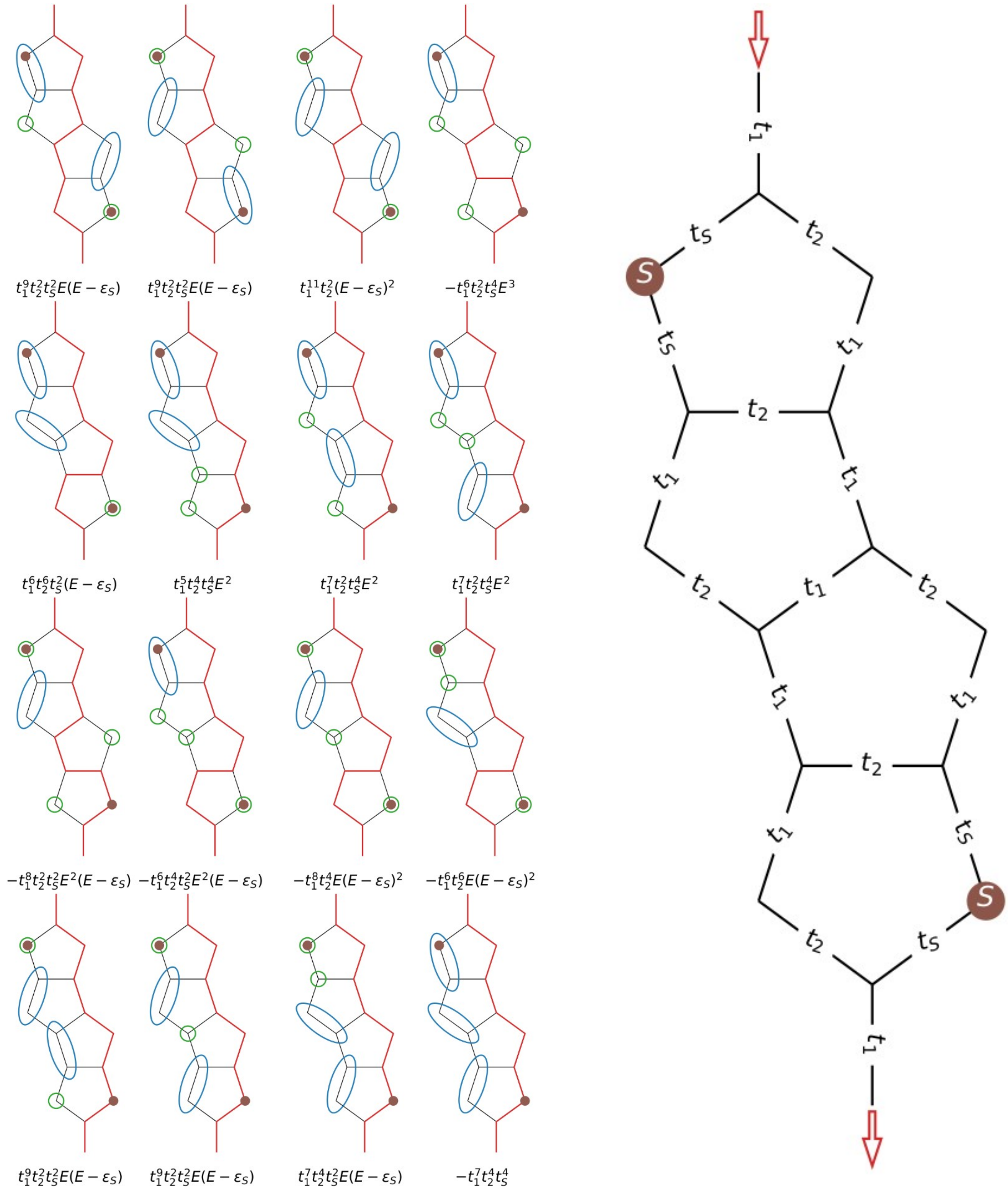

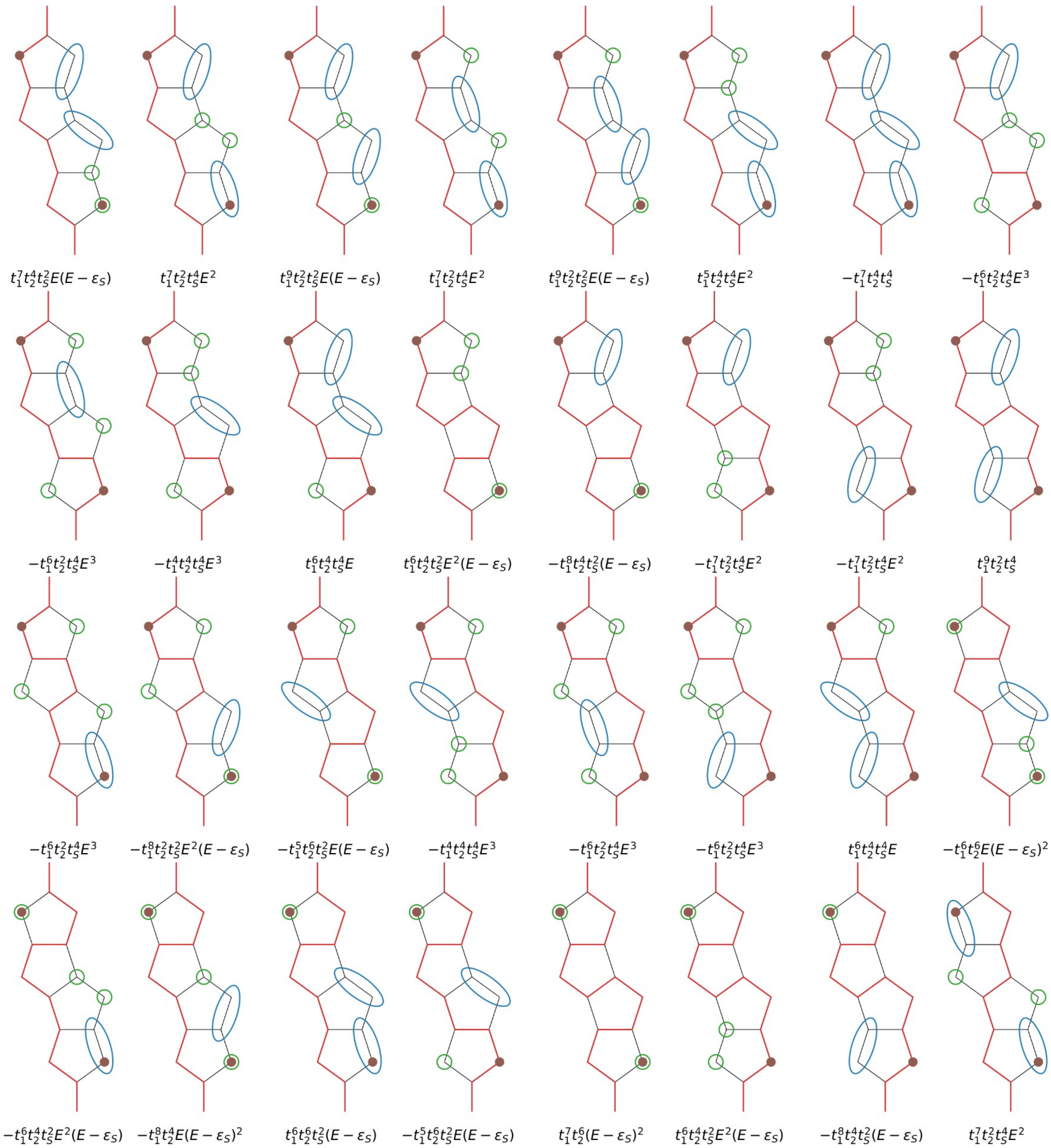

$t_1^7t_2^4t_S^2E(E-\varepsilon_S)$
$t_1^7t_2^2t_S^4E^2$
$t_1^9t_2^2t_S^2E(E-\varepsilon_S)$
$t_1^7t_2^2t_S^4E^2$
$t_1^9t_2^2t_S^2E(E-\varepsilon_S)$
$t_1^5t_2^4t_S^4E^2$
$-t_1^7t_2^4t_S^4$
$-t_1^6t_2^2t_S^4E^3$
$-t_1^6t_2^2t_S^4E^3$
$-t_1^4t_2^4t_S^4E^3$
$t_1^6t_2^4t_S^4E$
$t_1^6t_2^4t_S^2E^2(E-\varepsilon_S)$
$-t_1^8t_2^4t_S^2(E-\varepsilon_S)$
$-t_1^7t_2^2t_S^4E^2$
$-t_1^7t_2^2t_S^4E^2$
$t_1^9t_2^2t_S^4$
$-t_1^6t_2^2t_S^4E^3$
$-t_1^8t_2^2t_S^2E^2(E-\varepsilon_S)$
$-t_1^5t_2^6t_S^2E(E-\varepsilon_S)$
$-t_1^4t_2^4t_S^4E^3$
$-t_1^6t_2^2t_S^4E^3$
$-t_1^6t_2^2t_S^4E^3$
$t_1^6t_2^4t_S^4E$
$-t_1^6t_2^6E(E-\varepsilon_S)^2$
$-t_1^6t_2^4t_S^2E^2(E-\varepsilon_S)$
$-t_1^8t_2^4E(E-\varepsilon_S)^2$
$t_1^6t_2^6t_S^2(E-\varepsilon_S)$
$-t_1^5t_2^6t_S^2E(E-\varepsilon_S)$
$t_1^7t_2^6(E-\varepsilon_S)^2$
$t_1^6t_2^4t_S^2E^2(E-\varepsilon_S)$
$-t_1^8t_2^4t_S^2(E-\varepsilon_S)$
$t_1^7t_2^2t_S^4E^2$

References

[1] J. Usuba, M. Hayakawa, S. Yamaguchi, A. Fukazawa, Chemistry – A European Journal 2021, 27, 1638

[2] Pauly, F.; Viljas, J. K.; Huniar, U.; Häfner, M.; Wohlthat, S.; Bürkle, M.; Cuevas, J. C.; Schön, G. Cluster-Based Density-Functional Approach to Quantum Transport through Molecular and Atomic Contacts. New J. Phys. 2008, 10 (12), 125019.

[3] Zotti, L. A.; Bürkle, M.; Pauly, F.; Lee, W.; Kim, K.; Jeong, W.; Asai, Y.; Reddy, P.; Cuevas, J. C. Heat Dissipation and Its Relation to Thermopower in Single-Molecule Junctions. New J. Phys. 2014, 16 (1), 015004.

[4] Ahlrichs, R.; Bär, M.; Häser, M.; Horn, H.; Kölmel, C. Electronic Structure Calculations on Workstation Computers: The Program System Turbomole. Chem. Phys. Lett. 1989, 162 (3), 165–169.

[5] Schäfer, A.; Horn, H.; Ahlrichs, R. Fully Optimized Contracted Gaussian Basis Sets for Atoms Li to Kr. J. Chem. Phys. 1992, 97 (4), 2571–2577.

[6] Perdew, J. P. Density-Functional Approximation for the Correlation Energy of the Inhomogeneous Electron Gas. Phys. Rev. B 1986, 33 (12), 8822. (functional)

[7] Quek, S. Y.; Venkataraman, L.; Choi, H. J.; Louie, S. G.; Hybertsen, M. S.; Neaton, J. Amine−Gold Linked Single-Molecule Circuits: Experiment and Theory. Nano Lett. 2007,
7 (11), 3477–3482.

[8] L. J. O'Driscoll and M. R. Bryce, Nanoscale, 2021, 13, 1103–1123.